Femtosecond laser writing of robust waveguides in optical fibers with enhanced photosensitivity

L. Colliard, J. Lapointe, N. Grégoire, S. Morency, R. Vallée, Matthieu Bellec, M. Bernier

▶ **To cite this version:**

L. Colliard, J. Lapointe, N. Grégoire, S. Morency, R. Vallée, et al.. Femtosecond laser writing of robust waveguides in optical fibers with enhanced photosensitivity. Optics Express, 2024, 32 (11), pp.19735. ⟨10.1364/oe.521714⟩. ⟨hal-04702075⟩

HAL Id: hal-04702075

https://hal.science/hal-04702075v1

Submitted on 19 Sep 2024

HAL is a multi-disciplinary open access archive for the deposit and dissemination of scientific research documents, whether they are published or not. The documents may come from teaching and research institutions in France or abroad, or from public or private research centers.

L'archive ouverte pluridisciplinaire **HAL**, est destinée au dépôt et à la diffusion de documents scientifiques de niveau recherche, publiés ou non, émanant des établissements d'enseignement et de recherche français ou étrangers, des laboratoires publics ou privés.

HAL Authorization

Research Article | Vol. 32, No. 11 / 20 May 2024 / Optics Express 19735
Optics EXPRESS

Femtosecond laser writing of robust waveguides in optical fibers with enhanced photosensitivity

L. Colliard,[1,2] J. Lapointe,[1] N. Grégoire,[1] S. Morency,[1] R. Vallée,[1] M. Bellec,[2,*] and M. Bernier[1,3]

[1]Centre d'optique, photonique et laser (COPL), Université Laval, 2375 rue de la Terrasse, Québec, G1V 0A6, Canada
[2]Université Côte d'Azur, CNRS, INPHYNI, France
[3]martin.bernier@copl.ulaval.ca
[*]matthieu.bellec@univ-cotedazur.fr

Abstract: We report the femtosecond laser writing of meter-long optical waveguides inscribed through the coating of specifically designed optical fibers. In order to improve the material photosensitivity and to ensure non-guiding optical fibers for subsequent laser processing of the waveguiding core, a depressed refractive index core design is implemented by co-doping a large portion of the optical fiber with germanium oxide and fluorine. The enhanced photosensitivity provided by further deuterium loading these fibers allows laser-writing of large refractive index contrast waveguides over wide cross sections. To mitigate the formation of photoinduced color centers causing high propagation losses in the photo-written waveguides, thermal annealing up to 400°C is performed on polyimide-coated laser-written fibers. Although the refractive index contrast decreases, the propagation losses are drastically reduced down to 0.08 dB/cm at 900nm allowing a robust single-mode guiding from visible to near infrared. Our results pave the way towards the development of a new generation of optical fibers and photonic components with arbitrarily complex designs.

Published by Optica Publishing Group under the terms of the Creative Commons Attribution 4.0 License. Further distribution of this work must maintain attribution to the author(s) and the published article's title, journal citation, and DOI.

1. Introduction

When an ultrashort laser is strongly focused inside a transparent material, nonlinear absorption processes lead to microscale material property changes [1]. Such a direct-laser-writing (DLW) approach allows to process various integrated optical components in polymers [2], crystals [3] or glass materials [4] that are used in a broad range of photonic applications [5]. Beyond bulk materials, DLW is also highly suitable for optical fiber functionalization via additive fabrication [6] – a highly promising route for submicron-scale manufacturing of polymeric and glassy 3D complex photonic systems [7–12] – or via direct refractive index (RI) modifications [13]. The latter allows to fabricate, at a localized scale, optical fiber components such as fiber Bragg gratings (FBG) [14–17], waveguide-based interferometers and transducers [13,18–20] or optofluidic circuits for lab-on-fiber applications [21,22].

Moreover, reel-to-reel (R2R) laser writing configurations can be used to distribute optical functionalities over arbitrary long distances. For instance, distributed FBGs [23,24], laser-induced defects points [25] and continuous UV-induced defects [26,27] or femtosecond laser-induced type II (i.e. birefringent structures) RI modifications [28,29] have been implemented to enhance the scattering properties of optical fibers for distributed sensing applications. In addition, our group recently reported the DLW fabrication, directly through the coating, of few meters long low-loss waveguides in a coreless pure silica optical fiber [30]. To go one step further to the

#521714 https://doi.org/10.1364/OE.521714
Journal © 2024 Received 16 Feb 2024; revised 26 Apr 2024; accepted 30 Apr 2024; published 14 May 2024

Optics EXPRESS

development of on-demand waveguide-based complex architectures at the intermediate meter scale, it's necessary improve the light confinement, by increasing the refractive index modification and/or the waveguide cross section, in order to operate in the near-infrared (IR) while keeping low losses.

A common strategy to photoimprint high-efficiency FBGs with large refractive index contrasts (typically up to few 10^{-2}) is to enhance the optical fiber photosensitivity using germanium-oxide doped fiber core combined with hydrogenation processes. The presence of hydrogen or deuterium in the germanium-doped silica glass structure increases significantly the photoionization probability of the Ge-Ge and Ge-Si defect centers in the glass structure leading to a significant raise of the glass photosensitivity [31].

In this paper, following a similar approach to increase the RI contrast of the laser-written waveguides, we design large-core silica-based optical fibers co-doped with germanium-oxide (GeO_2) and fluorine (F_2) in order to result in a non-guiding depressed fiber core structure. Using the R2R phase-mask writing technique recently developed [30], we report the fabrication, directly through the fiber polymer coating, of meter long waveguides operating at low loss up to the near-infrared. We study the impact of deuterium loading these fiber samples and observe a clear increase of the RI contrast up to 6.10^{-3}. The photosensitivity increase allows, via a laser transverse scan during inscription, to fabricate a wide cross-section waveguide up to 8.4 μm in diameter. To mitigate the formation of photoinduced color centers that cause large propagation losses in the laser written waveguides, we performed a thermal annealing on the laser-written optical fibers coated with high temperature resistant polyimide. Although this process tends to reduce the refractive index contrast, we managed to achieve significantly better performance in terms of minimal losses compared to our previous work in pure silica [30] (a loss reduction of ~42% at 900 nm). More importantly we considerably improved the guiding properties of the resulting waveguide leading to much more robust waveguides with lower sensitivity to bending losses. To the best of our knowledge, this is the first report of meter-long waveguide inscription in such configuration which combines a reel-to-reel direct-laser-writing setup and specifically designed optical fibers. Our results pave the way towards the laser fabrication of robust and high-quality complex arrangements of arbitrarily long waveguides and photonics components (e.g. splitters, couplers, etc.) in optical fibers.

2. Experimental setup

2.1. Reel-to-reel direct-laser-writing system

Figure 1(a) illustrates the principle of the R2R-DLW configuration. The optical fiber is unwound, via a set of rotating spools and pulleys, at constant velocity v (ranging from 0.1 to 2 mm/s) along z and is exposed locally to a tightly focused IR ultrafast high-energy laser beam of 35 fs pulses and few 100 μJ at 800 nm and 1 kHz repetition rate (Coherent, Astrella). The longitudinal tension applied to the fiber is tuned to 4 N. The focusing stage, routinely used for FBGs fabrication [14], consists in an acylindrical lens (Thorlabs, AYL108-B, 8 mm focal length) and a 1070 nm uniform period phase-mask positioned at 200 μm from the center of the fiber. This allows to generate a 11 mm Gaussian-apodized sinusoidal interference pattern with 535 nm period and ~ 1×2 μm^2 cross section in pure silica glass [30]. The combination of the acylindrical lens and the phase mask reduces the spherical aberration in the transverse plane [32] and stabilizes the multifilamentation process [33] in the longitudinal plane. It therefore allows to distribute the writing beam over thousands of periodically arranged spots thus significantly speeding up the writing process to few mm/s. A conventional single spot writing from a focused circular beam at 1kHz would lead to a much lower writing speed to a few μm/s which would result in an overly long exposure of hundreds of hours to process a meter-long waveguide. It should also be noted that writing without phase-mask was tested and the fiber coating was damaged before any significant local refractive index modification could be induced as expected [33]. To further enlarge the focal cross section,

Optics EXPRESS

the acylindrical lens is mounted on a 2D piezoelectric scanner (PI, P-611XZ). Since the laser spot is slightly elongated along the y-axis, to obtain a quasi-circular refractive index distribution, the lens is moved along the x-axis at 4 Hz over few μm depending on the fiber composition. Note that above 12 μm range spherical aberrations lead to a deformed focal spot and inhomogeneous RI distribution. To overcome this limitation, beam shaping techniques (using e.g. cylindrical doublets [34] or a spatial light modulators [35]) adapted to our phase-mask setup [36] could be employed to compensate for the geometrical aberrations. The unwinding of the optical fiber during the writing process erases most of the grating periodicity, which ensures a continuous refractive index modification allowing the fabrication of smooth and homogeneous waveguides in the fiber. Typically, in a coreless pure silica optical fiber, we reported 2 μm wide waveguides with an almost circular cross-section [30]. The energy threshold of the prohibitive birefringent type II modifications leads to a little flexibility regarding the laser inscription parameters. Thus, to increase the refractive index change, we design optical fibers with enhanced photosensitivity.

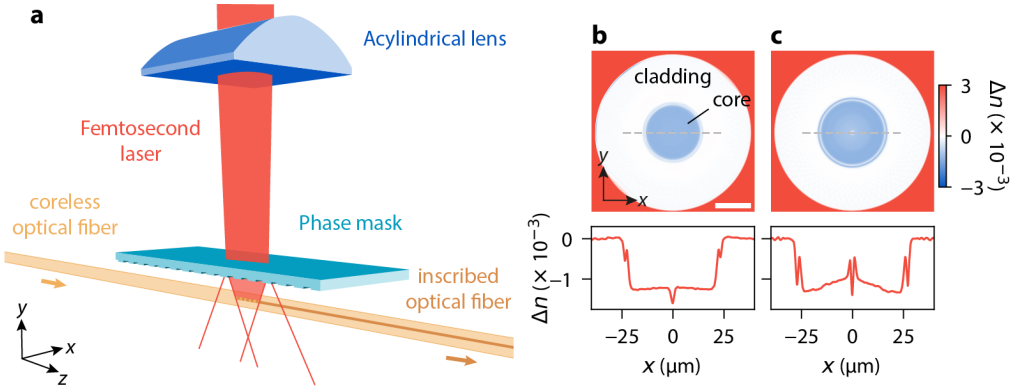

Fig. 1. (a) Sketch of the reel-to-reel direct-laser-writing experimental setup. The optical fiber is translated along z at constant velocity v and is locally inscribed via a DLW workstation which consists in a femtosecond laser beam focused from the side of the optical fiber, directly through the fiber coating, by an acylindrical lens combined with a phase-mask. The generated focal zone consists in an elongated sinusoidal pattern that is smoothed out during the fiber translation. (b, c) Experimentally measured transverse refractive index distributions with their corresponding profiles (plotted along the gray dashed line) of the $SiO_2/GeO_2/F_2$ co-doped silica fiber with low-GeO_2/F_2 concentration (b, cladding: pure silica, core: 98.3 mol% SiO_2, 0.9 mol% GeO_2, 0.8 mol% F_2) and higher-Ge_2/F_2 concentration (c, cladding: pure silica, core: 94.9 mol% SiO_2, 3.1 mol% GeO_2, 2.0 mol% F_2). The co-doped cores show a diameter of 52 μm and 61 μm respectively, and a similar refractive index decrease of $\sim -1.3 \times 10^{-3}$ respectively compared to the pure silica cladding. The white scale bar is 25 μm.

2.2. *Photosensitive optical fiber design and fabrication*

To enhance the glass photosensitivity while ensuring non-guiding properties of the resulting optical fiber to further process and adequately characterize the femtosecond-written waveguides, we co-doped a large portion of the silica glass fibers with GeO_2 and F_2.

Two preforms were successively fabricated using a modified chemical vapor deposition (MCVD) process by co-doping the SiO_2 sooth with GeO_2 and F_2 in the gaseous phase by adding $GeCl_4$ and fluorine to the $SiCl_4$ gas mixture during deposition. An optimized approach involving the deposition of very thin layers of sooth was implemented to ensure a smooth RI radial distribution, free of visible RI ripples, that would have resulted in significant inhomogeneity

Optics EXPRESS

during subsequent laser processing. The core/clad diameter ratio of both preforms was further adjusted to significantly increase the fiber core by etching the cladding using a bath of liquid HF.

The first preform was made as a proof of concept with a low doping concentration of 0.9 mol% GeO_2 and 0.8 mol% F_2. The amount of fluorine was adjusted to obtain a depressed RI core ensuring that the fiber was not guiding without any waveguide photo-inscribed. This depressed-core geometry is important in order to precisely characterize the photo-written waveguide properties by ensuring efficient light stripping by the fiber cladding and coating. This first preform was drawn into a 52/125 μm core/clad diameter optical fiber with a fiber tower adapted to silica glass drawing. The corresponding transverse refractive index distribution and profile are presented in Fig. 1(b). As compared to the pure silica cladding, the doped-core indeed exhibits a negative refractive index change of $\sim -1.3 \times 10^{-3}$. A standard polyacrylate coating was applied during the fiber drawing leading to an optical fiber with an external diameter of 250 μm.

The second preform was fabricated once the fiber resulting from the first preform was successfully photo-written and the resulting waveguiding properties characterized. To further enhance the material photosensitivity, this second preform was doped at higher concentration of 3.1 mol% GeO_2 and 2.0 mol% F_2. This preform was drawn into a 61/125 μm core/clad diameter optical fiber and also exhibits a negative refractive index change of $\sim -1.3 \times 10^{-3}$ compared to the pure silica cladding as shown in Fig. 1(c). The doping concentration in fluorine for the second preform was adjusted so that the resulting negative refractive index change of the doped core was approximately the same as for the first doped preform. Figure 1(c) shows that this higher doping concentration has led to a less uniform RI profile for the doped core compared with the first preform shown in Fig. 1(b).

As explained below, a polyimide coating was applied to this second fiber (leading to an external diameter of 134 μm) in order to mitigate, via thermal annealing, the photoinduced losses associated to the formation of color centers in the doped glass observed by characterizing the photo-written waveguides on the fiber from the first preform coated with standard polyacrylate. Such polyacrylate coating has a short-term operating temperature of only 150°C which is insufficient to anneal the color centers in germanosilicate fibers [37]. On the other hand, the polyimide coating is capable of withstanding short-term operating temperatures up to 400°C [38] which makes it a great choice to process the annealing of the fiber samples to mitigate the photoinduced losses during waveguide writing [37], and is expected to result in very low loss waveguides. It should be noted that removing the coating on the meter-long fibers to proceed with thermal annealing would have been a rather difficult option that we did not consider for practical reasons.

Finally, to further increase their photosensitivity, the two resulting optical fibers were loaded with deuterium at 2000 psi during 14 days. As a reference, we also considered a home drawn coreless pure silica fiber surrounded by a polyacrylate coating [30] before and after hydrogenation.

2.3. Waveguides characterization

The measurement of the transverse distribution of the refractive index is performed by an interferometric fiber analyzer (Interfiber Analysis, IFA-100). The longitudinal distribution of the optical path difference obtained with a wavefront sensor (Phasics, SID4Bio) attached to an optical microscope was also measured complementing the transverse RI characterization [39].

To obtain the propagation losses, first the spectral transmission was measured from 600 to 1200 nm for various laser-written waveguides of various lengths by coupling a supercontinuum source (Koheras, SuperK Power) to the waveguide input with an aspheric lens (New Focus, 5726-B) and by recording the transmitted signal with an optical spectrum analyzer (Yokogawa, AQ6370D). A reference single-mode fiber was used to normalize the transmission spectra. Then, the spectra are divided by the fiber length. For the cutback method, a set of transmission measurements was carried out after successively cutting a ~20cm piece of the laser-inscribed fibers. Fiber samples

Optics EXPRESS

were cut with a standard cleaver (CT50 Fujikura). If the cutting angle, checked with the angle calculator embedded in a fusion splicer (Fujikura 31S), is greater than 1°, the cleave was remade. Each measurement is averaged over multiple spectra. The corresponding error is ±1 dB. The propagation losses at a given wavelength are then obtained from a linear fit of the log scaled normalized transmission.

3. Results

3.1. Refractive index modification

We first investigated the laser-induced refractive index distribution of 12 cm-long waveguides inscribed in i) a pure silica optical fiber, ii) a D_2-loaded pure silica fiber, iii) a D_2-loaded GeO_2/F_2 fiber co-doped with low concentration and iv) a D_2-loaded GeO_2/F_2 fiber co-doped with higher concentration. The writing condition in terms of pulse energy and velocity are respectively i) 220 μJ, ii) 220 μJ, iii) 230 μJ and iv) 300 μJ at v = 1 mm/s each. The pulse energy is chosen to be slightly below the damage (type-II) threshold to ensure smooth type-I RI modifications ensuring low waveguiding losses and high fiber mechanical strength [40]. For the latter optical fiber, the polyimide coating requires a slightly stronger pulse energy considering its larger refractive index of $n \sim 1.7$ compared to $n \sim 1.55$ for polyacrylate [41]. We also increased the transversal range implemented by the piezoelectric actuator to design a larger cross section waveguide. Figure 2 presents the transverse refractive index distribution measured for each chemical composition (corresponding to each column). The first row displays the entire 125 μm diameter optical fibers while the second row focuses on the regions of interest delimited by the dashed gray boxes. The last row corresponds to the RI profiles along the dashed gray line. For the pure silica optical fiber, we obtained a maximum refractive index modification $\Delta n = (3.8 \pm 0.2) \times 10^{-3}$ with a full width at half maximum (FWHM) of 2.7 μm, in very good accordance to our previous work [30]. The D_2-loading process performed on the pure silica fiber allows to increase the Δn up to $(4.5 \pm 0.2) \times 10^{-3}$ with a slightly larger FWHM measured to 3.3 μm. For the D_2-loaded GeO_2/F_2 co-doped optical fiber at low doping concentration, the refractive index is greatly increased, up to $(5.7 \pm 0.2) \times 10^{-3}$ and the FWHM remains similar to the previous cases at 3.3 μm.

By varying the writing velocity, we conducted a more systematic study for the unloaded pure silica fiber, the D_2-loaded pure silica fiber and the D_2-loaded GeO_2/F_2 silica fiber co-doped at low concentration. As summarized in Fig. 3, we observed, as expected, a decrease of the maximum refractive index as v increases from 0.2 to 2 mm/s. Overall, compared to the results reported for a pure silica fiber [30] (gray curve), we measured a rise of 10% for the D_2-loaded pure silica (yellow curve) and of 35% for the D_2-loaded GeO_2/F_2 silica fiber co-doped at low concentration (red curve).

The GeO_2/F_2 co-doped D_2-loaded optical fiber at higher doping concentration with deuterium loading was not included in this systematic study because it was not available at that time. We observed a different behavior in this case shown in Fig. 2(d,h,l). The RI modifications were significantly lower for the laser parameters used with the previous polyacrylate coated optical fibers (i.e. 220-230 μJ) and a higher energy (300 μJ) were required to observe RI changes. We believe that due to the improved photosensitivity combined with the properties of the polyimide coating (reflexion losses, absorption and focusing conditions), the energy is deposited on a very elongated area requiring a large scanning sweep of the writing beam to maintain a quasi-circular cross section. The wide waveguide (8.4 μm FWHM) is thus counterbalanced by a rather low maximum Δn of $(3.1 \pm 0.2) \times 10^{-3}$ due to a significant spreading of the deposited energy. Lowering the writing speed or increasing the length of the elongated writing beam along the fiber (see Sec. 2.1) would have been required in this case to reach larger RI modifications, this will be the subject of an upcoming study. Figure 2(m) depicts the longitudinal distribution of the optical path difference (OPD) measured with a wavefront sensor (Phasics, SID4) attached to an optical microscope [39]. At this scale, the OPD is seems very homogeneous.

Optics EXPRESS

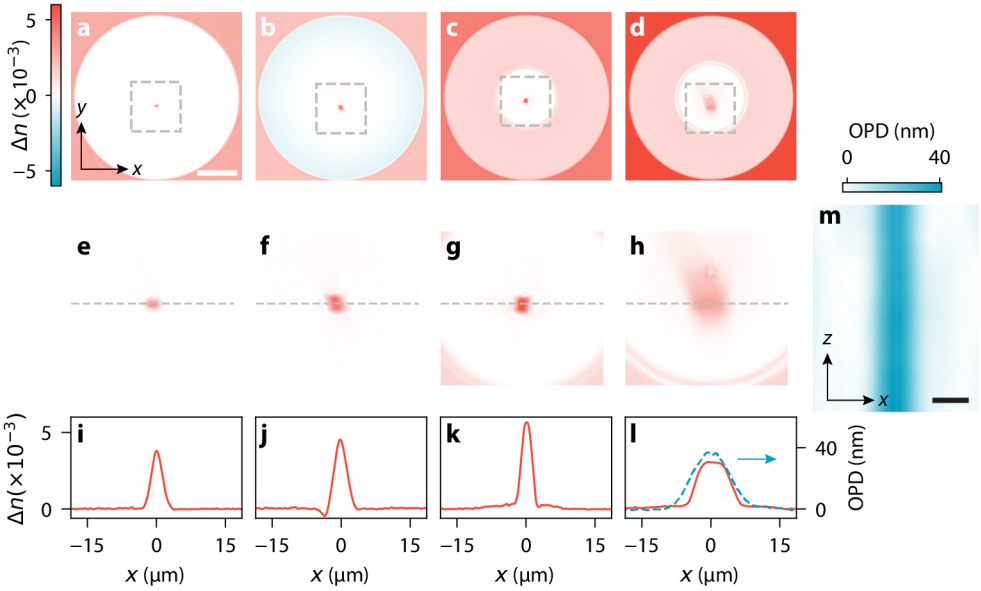

Fig. 2. Experimentally measured transverse refractive index distribution of 12 cm-long waveguides inscribed in four different optical fibers: a pure silica optical fiber (a), a D_2-loaded pure silica fiber (b), a D_2-loaded GeO_2/F_2 fiber co-doped with low concentration (c) and a D_2-loaded GeO_2/F_2 fiber co-doped with higher concentration (d). The writing pulse energy were 220 μJ, 220 μJ, 230 μJ and 300 μJ respectively and the velocity v = 1 mm/s. In (d), a larger scanning sweep of the writing beam was applied to maintain a quasi-circular cross section explaining the lower maximum RI change. The white scale bar is 30 μm. The second row (e–h) shows the corresponding regions of interest delimited by the dashed gray boxes in (a–d). The image size is 37 μm × 37 μm. The last row (i–l) shows the corresponding RI profiles delimited by the dashed gray lines in (e–h). (m) Longitudinal distribution of the optical path difference corresponding to the D_2-loaded GeO_2/F_2 fiber co-doped with higher concentration. The scale bar is 10 μm. The profile averaged along z is depicted by the dashed blue line in (l).

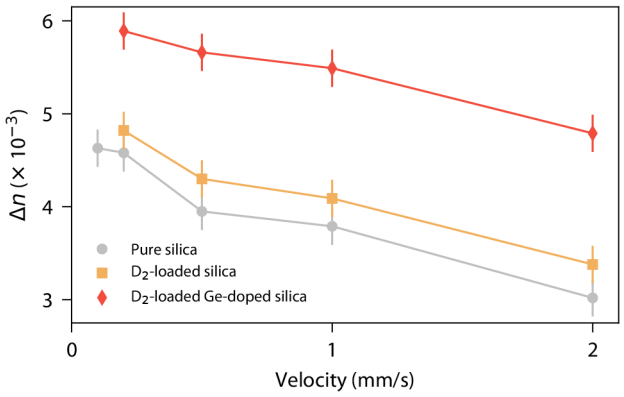

Fig. 3. Maximum refractive index modification Δn vs writing velocity v for three different optical fiber compositions: Unloaded pure silica (grey) D_2-loaded pure silica (yellow) and D_2-loaded GeO_2/F_2 fiber co-doped at low concentration (red). The gray curve is adapted from [30] and is provided for comparison.

Optics EXPRESS

3.2. Transmission measurements

To study the photo-written waveguide propagation losses, we implemented a cutback method on meter long waveguides inscribed in two different fibers (1.8 m in D_2-loaded GeO_2/F_2 silica fiber co-doped at low concentration and 0.94 m in D_2-loaded GeO_2/F_2 silica fiber co-doped at higher concentration). To do so, using a supercontinuum source and an optical spectrum analyzer, we measured the spectral transmission from 600 to 1200 nm for various waveguide lengths. Propagation losses were extracted by a fitting procedure. The results obtained at 900 nm which is close to the optimal transmission in both cases are summarized in Table 1. The losses are comparable to the (0.137 ± 0.002) dB/cm reported in pure silica [30] at the same wavelength. The refractive index increase and the wider waveguide cross section of the two fibers with low and high co-doping concentrations both lead to a better light confinement in the near-IR. That said, one should expect much lower propagation losses as well. This issue will be discussed in the next section.

Table 1. Propagation losses at 900 nm obtained from a cutback method performed on meter long samples for two different fibers (see the gray curve in Fig. 4(g) for the low GeO_2/F_2 concentration case). The error bars correspond to the standard deviation of fitted parameters. For comparison, the measurement at the same wavelength in pure silica optical fiber was (0.137 ± 0.002) dB/cm [30].

Fiber type	Losses (dB/cm)
GeO_2/F_2 low concentration	0.337±0.008
GeO_2/F_2 larger concentration	0.24±0.01

4. Discussions

In D_2-loaded co-doped optical fibers exposed to ultrashort IR laser pulses, the refractive index increase actually originates from both the glass densification and the formation of photoinduced color-centers [42]. Those color-centers are highly absorptive leading to detrimental propagation losses in the spectral range from UV up to near-IR [43]. In the framework of FBGs fabrication in H_2/D_2-loaded standard telecom germanosilicate fibers, it has been shown that an additional thermal annealing (typically up to 500°C) allows to suppress a large fraction of the photoinduced color-centers which is also accompanied by a ∼ 50% reduction of the refractive index change [42].

In this vein, we performed a thermal annealing on the laser-written waveguides (300 μJ, 1 mm/s) in the D_2-loaded GeO_2/F_2 silica fiber co-doped at higher concentration. As said previously, this fiber is protected by a polyimide coating that withstands high temperatures up to 400°C (in contrast to standard polyacrylate coating withstanding maximum temperatures of only 150°C). Figures 4(a–c) show the transverse refractive index distribution of a 12 cm-long waveguide written in such a fiber after the inscription (a), after a first thermal annealing at 200°C for 30 min (b) and after a last thermal annealing at 400°C for 30 min (c). As expected, the refractive index distribution remains similar but the maximum Δn drops almost linearly by 58% after the last thermal annealing, as depicted in the Fig. 4(d). This result is in very good accordance with the literature [42]. As observed in Figs. 2(d) and 4(a–c), the inscribed waveguides are not always perfectly centered in the large core. The fiber positionning instabilities likely come from the fiber slippage in the V-groove of the pulleys and from the mechanical noise of the motor managing the fiber tension [30]. The V-grooves were designed for standard polyacrylate coated optical fiber with 250 μm diameter. Since the polyimide coating was, by design, thinner than the standard polyacrylate one (4.5 μm compared to 65.5 μm, leading to a 134 μm diamater), the fiber slippage was larger and led to a higher deviation in the waveguide centering.

Optics EXPRESS

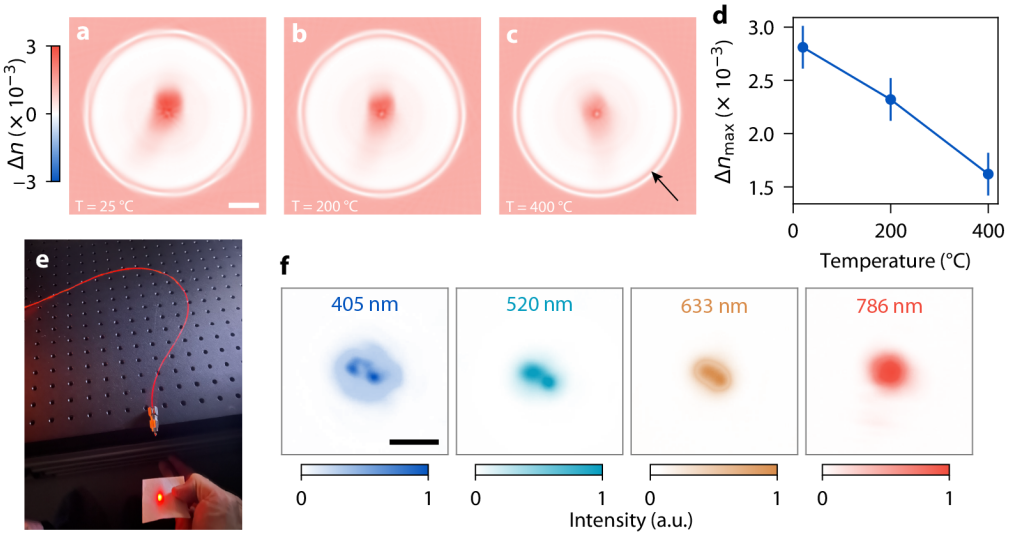

Fig. 4. (a–c) Transverse refractive index distributions of a 12 cm-long waveguide written in a D_2-loaded GeO_2/F_2 fiber doped at higher concentration at 300 μJ, 0.1 mm/s during a thermal annealing. (a) After the irradiation, (b) after a first thermal annealing at 200°C for 30 min and (c) after a last thermal annealing at 400°C for 30 min. The image size is 65 μm × 65 μm. The white scale bar is 10 µm. The black arrow in (c) indicates the first cladding structure. (d) Maximum refractive index change Δn_{max} vs the temperature. (e) Picture of the output signal when a supercontinuum source from 600 to 1200 nm is injected at the input of a 0.94 meter-long waveguide after the last thermal annealing. (f) Near-field intensity profiles measured at the output of the 12 cm-long waveguide (after the last thermal treatment at 400°C) measured for input wavelengths ranging from 405 to 786 nm. The scale bar is 20 µm.

The near-field intensity profile was measured at the output of the waveguide thermally annealed at 400°C for various input wavelengths ranging from 405 to 786 nm (using different laser diodes). The images presented in Fig. 4(f) show a clear single-mode behavior at 786 nm and suggest a wavelength cutoff between 633 and 786 nm. This is consistent with the theoretical value of 710 nm calculated by considering a 4μm-radius circular waveguide with a Δn of 1.55×10^{-3}.

Finally, the spectral transmission was measured from 600 nm to 1200 nm through a 0.94 m-long waveguide inscribed in the D_2-loaded GeO_2/F_2 fiber co-doped at higher concentration under the same conditions. The same thermal treatment was applied (200°C for 30 min and 400°C for 30 min). Note that the pure silica inscribed fiber previously studied [30] required to be held as straight as possible to limit the bending losses and transmit a guided signal. In comparison, as illustrated in Fig. 4(e), the 400°C thermally treated D_2-loaded GeO_2/F_2 fiber can be manipulated less carefully without any detrimental losses thus suggesting a more robust behavior regarding bending losses.

The output spectrum was measured as function of the annealing temperature, see Fig. 5(a). For the waveguide after inscription (blue curve), the optimal transmission was observed near 1075 nm with 0.15 dB/cm propagation losses. After a first thermal annealing (yellow curve), minimum losses of 0.10 dB/cm were measured at 1110 nm. As the annealing temperature increases (red curve), the losses drastically decreases in the short wavelength range, from 0.44 to 0.12 dB/cm at 700 nm and from 0.22 to as low as 0.08 dB/cm at 900 nm. This is confirmed by the propagation losses obtained from the cutback method performed on the thermally annealed fiber (Fig. 5(a), red circles). For instance, Fig. 5(b, red markers) depicts the normalized transmission measured

Optics EXPRESS

at 900 nm for various lengths of the waveguide inscribed in this fiber. The value obtained via a fitting procedure (red dashed line) is (0.08 ± 0.01) dB/cm. It is worth mentioning that the losses decrease with the wavelength in contradiction to what is observed with pure silica laser-inscribed fibers [30]. The loss mechanism might be different between the two types of optical fiber. In pure silica, propagation losses likely arise from the modal properties while it might come from scattering in the GeO_2/F_2 co-doped fibers. Note that for the optical fibers annealed at 400°C, the long wavelength guiding edge shifts down to 1000 nm (measurement artifacts above this wavelength were removed). Even if we suspect coupling to the cladding modes due to the decrease of the photoinduced refractive index, the deep understanding of the underlying loss mechanism is still under investigation. We are currently considering novel optical fiber designs with an adjusted GeO_2/F_2 ratio in the co-doped core to further increase the refractive index modification. Taking up this technological challenge would lead to femtosecond laser-inscribed waveguides with record low-losses of the order of a few dB/m in the near-IR. The proposed process is not yet suitable for km-long optical fibers. Besides losses, the writing velocity (of the order of mm/s) is also a limiting factor. It should be pointed out that increasing the input beam length or the repetition rate of the laser source used to write the waveguides could further speed up the writing process. Note that the latter configuration usually requires multiscan approach to achieve high contrast RI modifications (see e.g. [4,44,45]) which might not be compatible with our R2R setup. Laser-written waveguides would become highly suitable for the realization of innovative fibers having longitudinal varying core designs, on-demand fiber components such as splitters, couplers, or a complex arrangement of cores in few meters fibers. At rather short term, we aim at using beam shaping techniques (like e.g. [46]) to generate multiple spots in the transversal plane and implement integrated Mach-Zehnder interferometers by writing two cores with variable spacing and coupled chiral cores fibers by inscribing helical waveguides around an existing core in a standard single mode fiber.

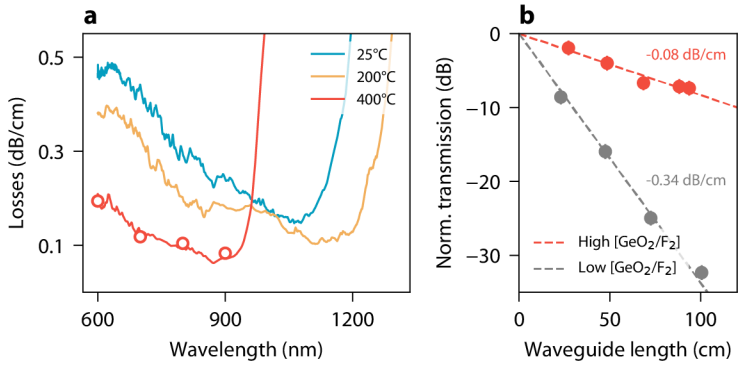

Fig. 5. (a) Propagation losses obtained by measuring the transmitted spectrum from 600 to 1200 nm after each thermal annealing steps performed on a 0.94 meter-long waveguide inscribed in the D_2-loaded GeO_2/F_2 fibers doped at high concentration. The red circles correspond to the losses measured by the cutback method at different wavelengths. The error bars, corresponding to the standard deviation of the fitted parameters, are similar to the marker sizes. (b) Normalized transmission measured at 900 nm for various waveguide lengths (cutback method) performed on the D_2-loaded GeO_2/F_2 fibers doped at low concentration (gray) and at higher concentration after the last annealing step (red). The error bars are similar to the marker sizes. The propagation losses are obtained via a linear fitting procedure (dashed lines).

Optics EXPRESS

5. Conclusions and perspectives

To conclude, using a reel-to-reel direct-laser-writing workstation, we have fabricated, directly through the coating, meter-long optical waveguides inside optical fibers. We specifically designed the optical fiber to improve the material photosensitivity and to ensure non-guiding optical fibers for subsequent laser processing of the waveguiding core. This has been done by co-doping a large portion of the optical fiber with germanium oxide and fluorine giving rise to a depressed refractive index core. The enhanced photosensitivity provided by further deuterium loading these fibers has allowed the laser inscription of waveguides with large refractive index contrasts over wide cross sections. To mitigate the formation of photoinduced color centers causing high propagation losses at short wavelength in the waveguides, thermal annealing up to 400°C has been performed on polyimide-coated laser-written fibers. Although the refractive index contrast decreases, the propagation losses have been drastically reduced down to 0.08 dB/cm at 900nm allowing a rather robust single-mode guiding in the near infrared. Our results pave the way towards the development of a new generation of low-loss optical fibers, potentially down to a few dB/m, and photonic components with arbitrarily complex designs.

Funding. Horizon 2020 Framework Programme (823941); Agence Nationale de la Recherche (ANR-15-IDEX-01); Canada Foundation for Innovation (5180); Fonds de recherche du Québec – Nature et technologies (114616, CO256655); Natural Sciences and Engineering Research Council of Canada (CRDPJ- 543631-19, IRCPJ469414-18, RGPIN-2016-05877); Canada First Research Excellence Fund (Sentinel North program).

Acknowledgments. The authors would like to thank P. Larochelle, T. Guérineau and S. Gagnon for technical assistance and L. Canioni for fruitful discussions.

Disclosures. The authors declare no conflicts of interest.

Data availability. Data underlying the results presented in this paper are not publicly available at this time but may be obtained from the authors upon reasonable request.

References

1. R. R. Gattass and E. Mazur, "Femtosecond laser micromachining in transparent materials," Nat. Photonics **2**(4), 219–225 (2008).
2. V. Harinarayana and Y. Shin, "Two-photon lithography for three-dimensional fabrication in micro/nanoscale regime: A comprehensive review," Opt. Laser Technol. **142**, 107180 (2021).
3. X. Xu, T. Wang, P. Chen, *et al.*, "Femtosecond laser writing of lithium niobate ferroelectric nanodomains," Nature **609**(7927), 496–501 (2022).
4. D. Tan, Z. Wang, B. Xu, *et al.*, "Photonic circuits written by femtosecond laser in glass: improved fabrication and recent progress in photonic devices," Adv. Photonics **3**(02), 024002 (2021).
5. M. Malinauskas, A. Žukauskas, S. Hasegawa, *et al.*, "Ultrafast laser processing of materials: from science to industry," Light: Sci. Appl. **5**(8), e16133 (2016).
6. A. Bertoncini and C. Liberale, "3d printed waveguides based on photonic crystal fiber designs for complex fiber-end photonic devices," Optica **7**(11), 1487 (2020).
7. X. Porte, N. U. Dinc, J. Moughames, *et al.*, "Direct (3+1)d laser writing of graded-index optical elements," Optica **8**(10), 1281–1287 (2021).
8. T. Doualle, J.-C. André, and L. Gallais, "3d printing of silica glass through a multiphoton polymerization process," Opt. Lett. **46**(2), 364–367 (2021).
9. C. R. Ocier, C. A. Richards, D. A. Bacon-Brown, *et al.*, "Direct laser writing of volumetric gradient index lenses and waveguides," Light: Sci. Appl. **9**(1), 196 (2020).
10. F. Kotz, K. Arnold, W. Bauer, *et al.*, "Three-dimensional printing of transparent fused silica glass," Nature **544**(7650), 337–339 (2017).
11. X. Wen, B. Zhang, W. Wang, *et al.*, "3d-printed silica with nanoscale resolution," Nat. Mater. **20**(11), 1506–1511 (2021).
12. J. Bauer, C. Crook, and T. Baldacchini, "A sinterless, low-temperature route to 3d print nanoscale optical-grade glass," Science **380**(6648), 960–966 (2023).
13. J. Zhao, Y. Zhao, Y. Peng, *et al.*, "Review of femtosecond laser direct writing fiber-optic structures based on refractive index modification and their applications," Opt. Laser Technol. **146**, 107473 (2022).
14. J. Habel, T. Boilard, J.-S. Frenière, *et al.*, "Femtosecond fbg written through the coating for sensing applications," Sensors **17**(11), 2519 (2017).
15. S. J. Mihailov, C. Hnatovsky, N. Abdukerim, *et al.*, "Ultrafast laser processing of optical fibers for sensing applications," Sensors **21**(4), 1447 (2021).

Optics EXPRESS

16. A. Martinez, I. Y. Khrushchev, and I. Bennion, "Direct inscription of bragg gratings in coated fibers by an infrared femtosecond laser," Opt. Lett. **31**(11), 1603 (2006).
17. A. Wolf, A. Dostovalov, K. Bronnikov, *et al.*, "Arrays of fiber bragg gratings selectively inscribed in different cores of 7-core spun optical fiber by ir femtosecond laser pulses," Opt. Express **27**(10), 13978 (2019).
18. J. R. Grenier, L. A. Fernandes, and P. R. Herman, "Femtosecond laser inscription of asymmetric directional couplers for in-fiber optical taps and fiber cladding photonics," Opt. Express **23**(13), 16760 (2015).
19. A. Rahnama, K. M. Aghdami, Y. H. Kim, *et al.*, "Ultracompact lens-less "spectrometer in fiber" based on chirped filament-array gratings," Adv. Funct. Mater. **1**, 2000026 (2020).
20. J. Han, Y. Zhang, C. Liao, *et al.*, "Fiber-interface directional coupler inscribed by femtosecond laser for refractive index measurements," Opt. Express **28**(10), 14263 (2020).
21. M. Haque, K. K. C. Lee, S. Ho, *et al.*, "Chemical-assisted femtosecond laser writing of lab-in-fibers," Lab Chip **14**(19), 3817–3829 (2014).
22. S. Pissadakis, "Lab-in-a-fiber sensors: A review," Microelectron. Eng. **217**, 111105 (2019).
23. F. Parent, S. Loranger, K. K. Mandal, *et al.*, "Enhancement of accuracy in shape sensing of surgical needles using optical frequency domain reflectometry in optical fibers," Biomed. Opt. Express **8**(4), 2210 (2017).
24. F. Monet, S. Loranger, V. Lambin-Iezzi, *et al.*, "The rogue: a novel, noise-generated random grating," Opt. Express **27**(10), 13895 (2019).
25. B. Redding, M. J. Murray, A. Donko, *et al.*, "Low-noise distributed acoustic sensing using enhanced backscattering fiber with ultra-low-loss point reflectors," Opt. Express **28**(10), 14638 (2020).
26. P. S. Westbrook, K. S. Feder, T. Kremp, *et al.*, "Integrated optical fiber shape sensor modules based on twisted multicore fiber grating arrays," in *Optical Fibers and Sensors for Medical Diagnostics and Treatment Applications XIV*, vol. 8938 (SPIE, 2014), p. 88.
27. P. S. Westbrook, K. S. Feder, T. Kremp, *et al.*, "Enhanced optical fiber for distributed acoustic sensing beyond the limits of rayleigh backscattering," iScience **23**(6), 101137 (2020).
28. M. Wang, K. Zhao, S. Huang, *et al.*, "Reel-to-reel fabrication of in-fiber low-loss and high-temperature stable rayleigh scattering centers for distributed sensing," IEEE Sens. J. **20**(19), 11335–11341 (2020).
29. M. Wang, K. Zhao, J. Wu, *et al.*, "Femtosecond laser fabrication of nanograting-based distributed fiber sensors for extreme environmental applications," Int. J. Extrem. Manuf. **3**(2), 025401 (2021).
30. L. Colliard, G. Bilodeau, T. Boilard, *et al.*, "Ultrafast laser writing of arbitrary long low-loss waveguides in optical fibers," Opt. Lett. **47**(23), 6253 (2022).
31. R. Kashyap, "Photosensitivity and photosensitization of optical fibers," in *Fiber Bragg Gratings*, (Academic Press, 2010).
32. P. Ji, S.-S. Lee, Y.-E. Im, *et al.*, "Determination of geometry-induced positional distortion of ultrafast laser-inscribed circuits in a cylindrical optical fiber," Opt. Lett. **44**(3), 610 (2019).
33. J.-P. Bérubé, R. Vallée, M. Bernier, *et al.*, "Self and forced periodic arrangement of multiple filaments in glass," Opt. Express **18**(3), 1801 (2010).
34. Y. Chen, Y. Lai, and M. W. O. Cheong, "Distortion-free femtosecond laser inscription in free-standing optical fiber," Appl. Opt. **55**(21), 5575–5579 (2016).
35. P. S. Salter, M. J. Woolley, S. M. Morris, *et al.*, "Femtosecond fiber bragg grating fabrication with adaptive optics aberration compensation," Opt. Lett. **43**(24), 5993–5996 (2018).
36. C. Voigtländer, R. G. Krämer, T. A. Goebel, *et al.*, "Variable wavefront tuning with a slm for tailored femtosecond fiber bragg grating inscription," Opt. Lett. **41**(1), 17–20 (2016).
37. L. Dong, J. L. Archambault, L. Reekie, *et al.*, "Photoinduced absorption change in germanosilicate preforms: evidence for the color-center model of photosensitivity," Appl. Opt. **34**(18), 3436 (1995).
38. K. Bronnikov, A. Wolf, S. Yakushin, *et al.*, "Durable shape sensor based on fbg array inscribed in polyimide-coated multicore optical fiber," Opt. Express **27**(26), 38421 (2019).
39. E. Bélanger, J.-P. Bérubé, B. de Dorlodot, *et al.*, "Comparative study of quantitative phase imaging techniques for refractometry of optical waveguides," Opt. Express **26**(13), 17498 (2018).
40. M. Bernier, F. Trépanier, J. Carrier, *et al.*, "High mechanical strength fiber bragg gratings made with infrared femtosecond pulses and a phase mask," Opt. Lett. **39**(12), 3646 (2014).
41. Y. P. Michel, M. Lucci, M. Casalboni, *et al.*, "Mechanical characterisation of the four most used coating materials for optical fibres," 2015 International Conference on Photonics, Optics and Laser Technology (PHOTOPTICS) **1**, 91 (2015).
42. M. Bernier, S. Gagnon, and R. Vallée, "Role of the 1d optical filamentation process in the writing of first order fiber bragg gratings with femtosecond pulses at 800nm," Opt. Mater. Express **1**(5), 832 (2011).
43. M. Lancry and B. Poumellec, "Uv laser processing and multiphoton absorption processes in optical telecommunication fiber materials," Phys. Rep. **523**(4), 207–229 (2013).
44. J. Lapointe, J.-P. Bérubé, S. Pouliot, *et al.*, "Control and enhancement of photo-induced refractive index modifications in fused silica," OSA Continuum **3**(10), 2851–2862 (2020).
45. B. Sun, F. Morozko, P. S. Salter, *et al.*, "On-chip beam rotators, adiabatic mode converters, and waveplates through low-loss waveguides with variable cross-sections," Light: Sci. Appl. **11**(1), 214 (2022).
46. Q. Geng, D. Wang, P. Chen, *et al.*, "Ultrafast multi-focus 3-d nano-fabrication based on two-photon polymerization," Nat. Commun. **10**(1), 2179 (2019).

134.59.89.217 on 2024-09-19 02:53:55